

*In the name of  
god*

*qcc.v*



دانشکده مهندسی

پایان نامه دکتری در رشته مهندسی مواد

تولید کامپوزیت های مغناطیسی نرم زمینه پلیمری و اندازه گیری  
خواص مغناطیسی آنها

۱۳۸۷ / ۲ / ۲۱

توسط

هومان شکراللهی

استاد راهنما

دکتر کمال جانقربان

دی ماه ۱۳۸۶

۹۳۳۵۷

مجلس اطلاعات در آن علمی بود  
توسعه در آن

دانشگاه شیراز



**Shiraz University  
Faculty of Engineering**

**Ph.D. Thesis  
In Materials Engineering**

**FABRICATION OF POLYMERIC-BASED SOFT  
MAGNETIC COMPOSITES AND MEASUREMENT OF  
THE MAGNETIC PROPERTIES**

**By  
HOOMAN SHOKROLLAHI**

**Supervised by  
KAMAL JANGHORBAN**

Jan. 2008

۱۳۸۷/۱۲/۲۵

دانشگاه شیراز  
فصلک

۲۰۰۸

IN THE NAME OF GOD

FABRICATION OF POLYMERIC-BASED SOFT MAGNETIC  
COMPOSITES AND MEASUREMENT OF THE MAGNETIC  
PROPERTIES

BY:

HOOMAN SHOKROLLAHI

THESIS

SUBMITTED TO THE SCHOOL OF GRADUATE STUDIES IN PARTIAL  
FULFILMENT OF THE REQUIREMENTS FOR THE DEGREE OF DOCTOR  
OF PHILOSOPHY (Ph.D.)

IN

MATERIALS SCIENCE AND ENGINEERING  
SHIRAZ UNIVERSITY  
SHIRAZ  
ISLAMIC REPUBLIC OF IRAN

EVALUATED AND APPROVED BY THE THESIS COMMITTEE AS:  
EXCELLENT

*Kamel Janghorban* K. JANGHORBAN, PROFESSOR OF MATERIALS  
SCIENCE AND ENGINEERING (CHAIRMAN)

*M.J. Hadianfard* M.J. HADIANFARD, ASSOCIATE PROF. OF MATERIALS  
SCIENCE AND ENGINEERING

*S. Javadpour* S. JAVADPOUR, ASSISTANT PROF. OF MATERIALS  
SCIENCE AND ENGINEERING

*M.H. PAYDAR* M.H. PAYDAR, ASSISTANT PROF. OF MATERIALS  
SCIENCE AND ENGINEERING

January 2008

## Acknowledgements

I would like to express my sincere gratitude to my supervisor, Professor Kamal Janghorban, outstanding educator, for his encouragement and care at all levels, and for his expert guidance and mentorship in my professional development. He had a decisive influence over my life and my future, giving me the opportunity to work in his research area. Without his support and the support of the following people, this work would not have been completed.

I would like to thank Dr. M.J. Hadianfard, Dr. S. Javadpour and Dr. M.H. Paydar, who acted as my thesis committee and gave me encouraging and helpful advises, and Dr. Maddah Hoseini from Sharif University and Dr. H. Abiri for their scientific comments and expertise.

I want to thank Dr. A. Tcharkhtchi in Ecole of ENSAM in Paris, who invited me to France, for doing some experiments and for the useful discussions on polymers. A special thank to Dr. F. Mazaleyrat and Dr. M. Lo Bue in Ecole of Cachan in south of Paris for their discussions throughout the experimental work and for technical assistance and data analysis.

I would like to express my special thanks and gratitude to my parents, for their love, patience, and understanding and for the wonderful moments we spent together in the last six years while I worked on my PhD program, providing me a warm and family environment.

I am thankful to all my friends for their support, and to the personnel of the Materials Science Laboratory, especially Mrs. Kaveh, Mr. Ghahremani, Mrs. Monsef, Mr. Dehghanian, Mr. Semati, and Mr. Maleksaeedi for their help.

Financial support from Fars Technical Research Commission and Shiraz University Research Council and office of the Kar-afariny (work-opportunity) is highly acknowledged. Some magnetic measurements were performed at the Magnetic Research Lab. Group, Tabriz University, which is appreciated.

## Abstract

### FABRICATION OF POLYMERIC-BASED SOFT MAGNETIC COMPOSITES AND MEASUREMENT OF THE MAGNETIC PROPERTIES

By:

Hooman Shokrollahi

Iron powder with high purity was covered by a polyepoxy, DDS and DGEBA (4,4'-Diaminodiphenyl Sulfone,  $C_{12}H_{12}N_2O_2S$ , and Diglycidyl Ether of Bis Phenol A) and effect of amount of resin, different curing treatments and compaction pressure on the magnetic properties, residual stresses, densification and microstructure were examined. Results showed that the samples with double insulation layers of phosphate and polyepoxy had minimum power loss. Also, the sample with 3wt% polyepoxy compacted at 800MPa had an acceptable real part of permeability and minimum imaginary part of permeability in comparison with other samples. Partial curing treatment reduced the imaginary part of permeability; and annealing treatment reduced this part of permeability and increased the real part of permeability. The permeability of small-size particles, 30  $\mu m$ , was lower than that of large-size particles, 100 $\mu m$  and 50 $\mu m$ , at low frequencies (<200 Hz) and was higher than that of large-size particles at high frequencies (>200 Hz). The permeability value for the sample with a diameter about 30 $\mu m$  was higher than (35%) that of the sample with 100 $\mu m$  diameter. Compaction experiments showed that increasing the pressure and applying warm compaction and two-step compaction methods for iron powders increased the magnetic induction and density and decreased the core loss. Different annealing (two steps annealing and magnetic annealing) treatments were applied to some samples. It was found that at low frequencies (<10kHz) the magnetic loss in the high-temperature magnetic annealed state (280°C/0.5T) was smaller than that in the low-temperature magnetic annealed (180°C/0.5T) and without annealing state. On the contrary, the magnetic loss in the high-temperature magnetic annealed state was larger at high frequencies (>10kHz) than the others. The results showed that magnetic loss of annealed powder was smaller than that of unannealed powder after 100 hours milling process. By loss separation technique ( $P/f=C_0+C_1f+C_2f^{1/2}$ ), different magnetic losses and the related coefficients for two different composites including single insulation layer (iron phosphate) and double insulation layer (iron phosphate+polyepoxy) were calculated. The results showed that the sample with double layer coating had lower bulk eddy currents.

## Table of Contents

Content	Page
Abstract.....	III
Chapter 1.....	1
Introduction.....	1
Chapter 2.....	6
Literature Review.....	6
Chapter 3.....	9
Theory.....	9
3.1. Material structure.....	9
3.2. Magnetization.....	10
3.3. Hysteresis.....	14
3.3.1. Domain boundary movement.....	16
3.3.2. Domain rotation.....	16
3.4. Magnetic Energies.....	17
3.4.1. Exchange Energy.....	17
3.4.2. Crystalline Anisotropy Energy.....	18
3.4.3. Dipole-Dipole Energy.....	18
3.4.4. Substrate and Surface Energies.....	20
3.5. Coercivity.....	20
3.6. Magnetic permeability.....	21
3.6.1. Relative permeability ( $\mu_r$ ).....	22

Content	Page
3.6.2. Initial permeability ( $\mu_i$ ) .....	22
3.6.3. Amplitude permeability ( $\mu_a$ ) and maximum permeability ( $\mu_m$ ) .....	22
3.6.4. Reversible or incremental permeability ( $\mu_{rev}$ , $\mu_\Delta$ ) .....	23
3.6.5. Apparent permeability ( $\mu_{app}$ ) .....	24
3.6.6. Effective magnetic permeability ( $\mu_e$ ) .....	24
3.6.7. Complex Permeability .....	24
3.7. Permeability and permittivity in composite media .....	27
3.8. Magnetic losses .....	28
3.8.1. Static loss (Hysteresis loss) .....	31
3.8.2. Eddy current loss .....	32
3.8.3. Excess loss .....	35
3.9. Soft magnetic composites and their applications .....	38
Chapter 4 .....	40
Procedure Method .....	40
4.1. Materials selection .....	41
4.2. Coating process .....	41
4.2.1. Inorganic coating .....	41
4.2.2. Phosphating treatment .....	42
4.3. Compaction .....	42
4.4. Annealing .....	43
4.4.1. Two steps annealing .....	43
4.4.2. Magnetic annealing .....	43
4.5. Measurements .....	44
4.5.1. Microstructural studies .....	44



<b>Content</b>	<b>Page</b>
4.5.2. Lattice parameter, crystallite size and microstrain .....	44
4.5.3. Bulk surface residual stresses .....	Error! Bookmark not defined.
4.5.4. Magnetic properties .....	Error! Bookmark not defined.
Chapter 5 .....	47
Results and Discussion.....	47
5.1. Iron powders coated with an iron phosphate and a polyepoxy .....	47
5.1.1. Experimental method .....	47
5.1.2. Phosphate layer characterisation .....	48
5.1.3. Densification and microstructural studies .....	49
5.1.5. Magnetic characteristics.....	55
5.2. Warm compaction.....	61
5.2.1. Experimental method .....	61
5.2.2. Results and discussion .....	61
5.3. Annealing.....	67
5.3.1. Experimental methods.....	67
5.3.2. Results and discussion .....	68
5.4. Eddy current loss in powder and laminated materials.....	77
5.4.1. General concepts .....	77
5.4.2. Eddy current loss in a laminated material.....	79
5.4.3. Eddy current loss in metallic powder particles .....	81
5.4.4. Eddy current loss in a cylinder .....	83
5.4.5. Total eddy current loss in an iron powder material .....	84
5.4.6. Eddy current loss in two soft magnetic composites.....	85
Chapter 6 .....	88

**Content**

**Page**

**Conclusions and Recommendations** .....88

**6.1. Conclusions** .....88

**6.2. Recommendations** .....90

**List of publications** .....99

## List of Tables

Table	Page
Table 1.1. Some of the thermosets which are used for coating.....	3
Table 1.2. Parameter dependence on composition and the fabrication process.....	4
Table 2.1. Literature survey in the field of soft magnetic composite materials.....	7
Table 4.1. Distribution size, physical property and chemical analysis for iron powder with high purity (WPL-200). .....	41
Table 5.1. Different curing treatments for the sample with 3 wt% of polymer. ....	48
Table 5.2. Density at different compaction temperatures (P=800 MPa).....	62
Table 5.3. Magnetic properties after heat treatment. ....	67
Table 5.4. Magnetic properties for three different particle sizes at 1200 MPa. ....	67
Table 5.5. The effect of heat treatment on the magnetic properties (D=30 $\mu$ m and f=200 Hz). .....	67
Table 5.6. Powders prepared by different milling and annealing conditions.....	68
Table 5.7. Lattice strain for powders with different milling-annealing condition. ....	71
Table 5.8. Particle size, effective radius and electrical resistivity for iron, and iron with different coatings. ....	86
Table 5.9. Total eddy current loss coefficient for two SMCs.....	86

## List of Figures

Figure	Page
Fig. 1.1. The applicable regions for soft magnetic materials used in AC magnetic fields.....	2
Fig. 1.2. A schematic diagram of the component elements of a powder core [65].....	2
Fig. 1.3. The total losses for ring shaped components with un-coated and coated iron powder particles.....	2
Fig. 1.4. Initial flux density curves for two iron specimens: (a) 99.9% pure Fe; (b) 99.99% pure Fe. ....	4
Fig. 2.1. Commercial ABS motor; a) Original Laminated motor, b) Improved new SMC design [65]. ....	8
Fig. 3.1. Iron crystal with BCC-structure and magnetization directions, easy $\langle 100 \rangle$ , medium $\langle 110 \rangle$ and hard $\langle 111 \rangle$ [89]. ....	10
Fig. 3.2. Continuously change of dipole alignment in an $180^\circ$ domain wall [89].....	10
Fig. 3.3. Aligned atomic dipoles in an external field. ....	12
Fig. 3.4. A simplified representation of the magnetizing processes and the corresponding initial magnetizing curve [12]. ....	12
Fig. 3.5. Different steps of magnetization [128]. ....	15
Fig. 3.6. Two hysteresis loops for soft and hard magnetic materials [12]. ....	15
Fig. 3.7. Broken spherical symmetry with formation of easy magnetization axis [129]. ....	17
Fig. 3.8. Various types of permeabilities, maximum permeability, $\mu_m$ , initial permeability, $\mu_i$ , and incremental permeability, $\mu_\Delta$ . The remanence $B_r$ and coercivity $H_C$ are also marked. ....	23
Fig. 3.9. Phase angle between magnetic induction and magnetic field strength [133]. ....	25
Fig. 3.10. Real and imaginary components of initial complex relative permeability versus frequency. Data were obtained from a Mn-ferrite [130]. ....	26

<b>Figure</b>	<b>Page</b>
Fig. 3.11. Effect of particle size on initial permeability [107].	26
Fig. 3.12. Loss per cycle and unit mass in a nonoriented Si-Fe lamination, 0.21 mm thick. Measurements were made under sinusoidal induction of 1.5 T peak value [129].	29
Fig. 3.13. Core loss versus frequency for the iron powder material at the sinusoidal peak flux densities of 0.5 T, 1 T and 1.5 T [92].	30
Fig. 3.14. Scheme of the pinning process of a domain wall by a nonmagnetic inclusion (left hand). Arrows indicate the wall velocity. On the right hand is shown the wall velocity profile within the axis of the inclusion [133].	32
Fig. 3.15. Field and current orientation in an infinite conducting plate [133].	34
Fig. 3.16. Dynamic wall bowing [133].	37
Fig. 3.17. Concept for iron loss reduction [63].	38
Fig. 4.1. Sample preparation flow chart [77].	40
Fig. 4.2. Equivalent circuit of inductors. (a) Lumped parameter equivalent circuit. (b) Simplified equivalent circuit for $R_c \ll R_{ac}$ . (c) Series equivalent circuit. (d) Equivalent circuit assumed by many LCR meters [134].	46
Fig. 4.3. Equivalent series resistance $R_s$ of the experimentally tested inductor. -.- calculated; o-o-o- measured [134].	46
Fig. 5.1. Composition as determined with energy-dispersive analysis (EDX) in the scanning electron microscope (SEM) of phosphated iron powders. Note the presence of the phosphorus peak. Accelerating Voltage: 15.0 kV and Magnification: 180.	49
Fig. 5.2. Effect of compaction pressure on the density of samples with different wt% of polyepoxy. compaction before curing ( $\square$ at $T=25.5^\circ\text{C}$ ).	50
Fig. 5.3. A comparison between densities different for samples with 3wt% polyepoxy compacted at different pressures ( $\square$ at $T=25.5^\circ\text{C}$ ).	50
Fig. 5.4. SEM images of surface of the SMC material (3wt% polyepoxy, compacted before final curing at 1138 MPa) in direction of applied pressure (a) interparticle connection with epoxy, (b) interparticle connection without epoxy, (c) and (d) epoxy accumulation.	51
Fig. 5.5. Composition as determined with energy-dispersive analysis (EDX) in the scanning electron microscope (SEM) of polyepoxy coated iron powders. Note the presence of the carbon peak. Voltage: 10.0 kV and Magnification: 900.	52

<b>Figure</b>	<b>Page</b>
Fig. 5.6. SEM images of surface of the SMC material (3wt% polyepoxy, compacted after curing at 1138 MPa) in direction of applied pressure. (a) and (b) particle separation, (c) particle separation at high magnification and (d) fracture surface.....	52
Fig. 5.7. Compressive residual stresses ( $-\sigma$ ) as a function of compaction pressure for iron-based samples with different wt% of polyepoxy, compaction before curing. ....	53
Fig. 5.8. Integral peak width as a function of compaction pressure for iron-based samples with different wt% of polyepoxy, compaction before curing. ....	54
Fig. 5.9. Compressive residual stresses ( $-\sigma$ ) as a function of compaction pressure for iron-based samples (3wt% DDS+DGEBA).....	54
Fig. 5.10. Evolution of integral Peak width as a function of compaction pressure for iron-based samples (3wt% DDS+DGEBA).....	55
Fig. 5.11. Variation of real part of permeability with frequency for two samples (P=380 MPa). Inorganic coating (phosphate coating, Fe-P).....	57
Fig. 5.12. Variation of imaginary part of permeability with frequency for two different samples (P=380 MPa). Inorganic coating (phosphate coating, Fe-P).....	57
Fig. 5.13. Real part of permeability in static form as a function of compaction pressure and polyepoxy content wt%.....	58
Fig. 5.14. Real part of permeability in static form as a function of different thermal treatments.....	58
Fig. 5.15. Imaginary part of permeability as a function of compaction pressure and polyepoxy content wt% (at $f=f_r$ ). ....	59
Fig. 5.16. Imaginary part of permeability as a function of compaction pressure for samples with different thermal and curing treatments (at $f=f_r$ ).....	60
Fig. 5.17. Resonance-relaxation frequency as a function of polyepoxy content wt% and compaction pressure.....	60
Fig. 5.18. SEM micrographs for different samples compacted at different temperatures A: 550°C, B: 350°C and C: room temperature (P=800 MPa). ....	62
Fig. 5.19. Magnetic loss as a function of silicone content at $f=10$ kHz for compacted samples at 800 MPa and room temperature.....	63

<b>Figure</b>	<b>Page</b>
Fig. 5.20. Magnetic loss as a function of frequency (logarithmic level) for compacted samples with and without silicone adhesive (P=800MPa).....	63
Fig. 5.21. Magnetic loss as a function of frequency at high frequencies for compacted samples with and without silicone adhesive (P=800MPa).....	64
Fig. 5.22. Equivalent series resistance as a function of frequency in logarithmic level (P=800MPa).....	64
Fig. 5.23. Magnetic permeability as a function of frequency (P=800MPa).....	65
Fig. 5.24. Magnetic loss as a function of frequency (logarithmic level) for compacted samples with silicone adhesive (P=800MPa).....	65
Fig. 5.25. Strength of green compacts for warm and cold compacted materials (P=800MPa). .....	66
Fig. 5.26. SEM micrographs for two different powders, A: series 1 and B: series 4.....	69
Fig. 5.27. X-ray diffraction patterns of four different powders, A: Series 4, B: Series 3, C: Series 2 and D: Series 1. ....	70
Fig. 5.28. Equivalent series resistance as a function of frequency (logarithmic level) at low frequencies. ....	71
Fig. 5.29. Magnetic permeability as a function of frequency at low frequencies. ....	72
Fig. 5.30. Magnetic loss as a function of frequency (logarithmic level) at low frequencies. .	72
Fig. 5.31. SEM micrographs of iron powders, (A) unmilled powder and (B) milled powder for 50 hours. ....	73
Fig. 5.32. Equivalent series resistance as a function of frequency (logarithmic level) between 0.1-100 kHz.....	74
Fig. 5.33. Equivalent series resistance as a function of frequency (logarithmic level), high frequencies (>10kHz).....	74
Fig. 5.34. SEM micrographs for the sample (A) without annealing treatment (B) magnetic annealing at 0.5 T/280°C for 300S.....	74
Fig. 5.35. Magnetic loss as a function of frequency (logarithmic level) at low frequencies (<10kHz).....	75
Fig. 5.36. Magnetic loss as a function of frequency at high frequencies (>10kHz). ....	76

<b>Figure</b>	<b>Page</b>
Fig. 5.37. Magnetic permeability as a function of frequency at low frequencies. ....	77
Fig. 5.38. The magnetic field and the selected element inside a laminate. ....	79
Fig. 5.39. A magnetic field applied to the sphere particle. ....	81
Fig. 5.40. Many spheres inside a laminate material. ....	82
Fig. 5.41. Behavior of the loss per cycle vs. the magnetizing frequency, measured on two SMCs, at a peak magnetization 0.05 T (P=400 MPa). The filled lines represent the best fit curve obtained from loss separation equation. ....	86
Fig. 5.42. Frequency dependence of $P_e$ for samples compacted at 400 MPa and B=0.05 T...	87



## List of Symbols

Symbols	Designation
I	Current
Q	Quality factor
f	Frequency
$P_t$	Total power loss
$P_h$	Hysteresis loss
$P_e$	Eddy current loss
L	Self inductance
$\mu_0$	Absolute permeability
$\mu_i$	Initial permeability
$\mu_e$	Effective permeability
$\mu_m$	Maximum permeability
$\mu_c$	Complex permeability
$\mu_r$	Relative permeability
$\mu_s$	Saturation permeability
$\mu_{app}$	Apparent permeability
M	Saturation magnetization
R	Resistivity
$\rho$	Resistivity of core material
B	Flux density
$B_r$	Remanent flux density
$B_e$	Effective flux density
$B_s$	Saturation flux density

H	Magnetic field strength
$H_C$	Coercive magnetic field strength
$H_i$	Internal magnetic strength
$\gamma$	Gyromagnetic ratio
$\alpha$	Magnetostriction coefficient
$\lambda$	Magnetocrystalline coefficient
T	Temperature
$T_C$	Curie temperature
$T_N$	Neel temperature
k	Susceptibility
l	Length
$K_B$	Boltzmann's constant
$\tan \delta$	Loss factor
$K_1$	Magneto-crystalline anisotropy
a	Lattice parameter
$\gamma_w$	Wall energy

## Chapter 1 Introduction

During the last several years, interest in the study of Soft Magnetic Composites (SMCs) has been increasing at an accelerating rate, stimulated by recent advances in materials synthesis and characterization techniques and the realization that these materials exhibit many unique and interesting physical and chemical properties with a number of potential technological applications. These composite materials offer several advantages over traditional laminated steel cores in most applications. The unique properties include three-dimensional (3D) isotropic ferromagnetic behavior, very low eddy current loss, relatively low total core loss at medium and high frequencies, possibilities for improved thermal characteristics, flexible machine design and assembly and a prospect for greatly reduced weight and production costs. Figure 1.1 shows the applicable regions for several soft magnetic materials used in AC magnetic fields. Soft ferrite has low core loss in the high frequency region, but due to its low magnetic flux density, it has the drawback of requiring a large core. Electrical steel sheets have high flux density, but electrical sheets cannot be used in the high frequency region due to the excessive core loss. Powder cores are magnetic materials which cover the region where the former two magnetic materials cannot be used.

SMCs, which are used in electromagnetic applications, can be described as ferromagnetic powder particles or soft magnetic powders surrounded by an electrical insulating film (Fig. 1.2). This insulating film can reduce the eddy currents at relatively high frequencies. Figure 1.3 shows the ring shaped component with coated iron powder exhibits lower power loss. The magnetically soft powders must combine as many as possible of the following characteristics at moderate cost: (1) low hysteresis losses, (2) low eddy current losses, (3) high permeability at low field strength, (4) high saturation value, (5) no aging effects and (6) uniform magnetic characteristics.

Insulation materials used for SMCs can be divided into two categories: organic and inorganic materials. Inorganic coatings can be subdivided into several categories; metallic oxide coatings (such as,  $\text{Fe}_2\text{O}_3$ ), phosphate coatings (zinc phosphate, iron phosphate and manganese phosphate), and sulfate coatings. Organic coatings can be subdivided into three categories, thermoplastic coatings, elastomers and thermosetting coatings. Thermoset resins have several advantages over thermoplastic and elastomeric materials. The selection of a thermoset instead of a thermoplastic is done to minimize the effect of the temperature variations on the magnetic and mechanical properties of the composites. Some of the thermosets which are used for coating are listed in table 1.1.

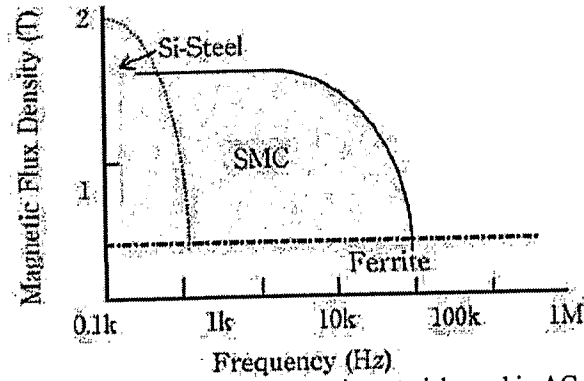


Fig. 1.1. The applicable regions for soft magnetic materials used in AC magnetic fields.

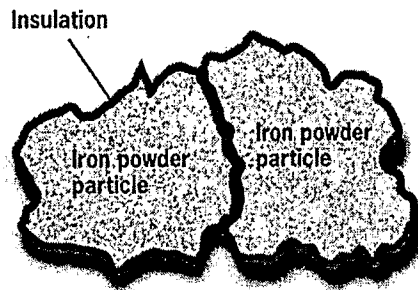


Fig. 1.2. A schematic diagram of the component elements of a powder core [65].

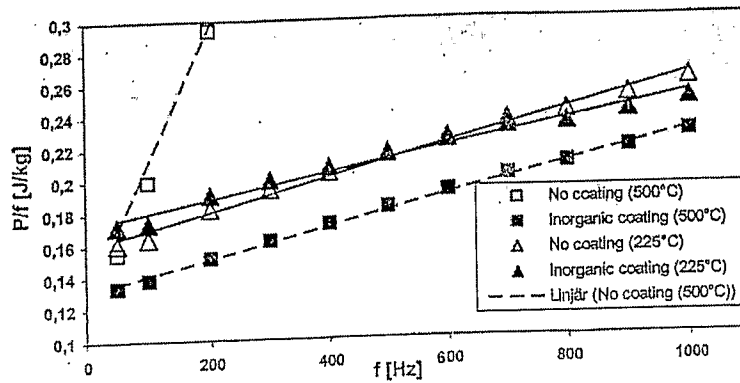


Fig. 1.3. The total losses for ring shaped components with un-coated and coated iron powder particles.